Ultrathin Films of Poly(ethylene oxides) on Oxidized Silicon. 2. In Situ Study of Crystallization and Melting by Hot Stage AFM

Holger Schönherr*,† and Curtis W. Frank*

NSF MRSEC Center on Polymer Interfaces and Macromolecular Assemblies (CPIMA) and Department of Chemical Engineering, Stanford University, Stanford, California 94305-5025

Received May 6, 2002; Revised Manuscript Received December 5, 2002

ABSTRACT: We report on the isothermal crystallization behavior of thin (film thickness d < 500 nm) and ultrathin (d < 100 nm) films of poly(ethylene oxide) (PEO), as well as pyrene end-labeled PEO, on native silicon studied by in situ hot stage atomic force microscopy (AFM). Individual lamellae were imaged during crystallization and melting. Using AFM, we have directly measured lamellar growth rates, lamellar thicknesses, and melting ranges as a function of film thickness (ca. 15−>500 nm), crystallization temperature (40−62 °C), and molar mass (11−100 kg/mol). On the basis of the Hoffman−Weeks extrapolation, the Gibbs−Thomson equation, and the Hoffman−Lauritzen theory, we show that the crystallization of PEO in thin and ultrathin films can be described with the same laws as the bulk crystallization. In addition, we find that the equilibrium melting points and surface free energies of the fold surfaces agree quantitatively with literature data for bulk crystallization and hence are not altered due to confinement in ultrathin films. However, there is a monotonic decrease of lamellar growth rates with decreasing film thickness for films thinner than ca. 250 nm. The growth rates decrease to below 1% of their bulk value in the thinnest films; this is attributed to an increase in glass transition temperature of up to 30 °C for the confined PEO and the concomitant reduction of molecular mobility.

Introduction

The confinement of polymers in ultrathin films (thickness < 100 nm),[1,2] block copolymers, or nanocomposites is known to significantly alter numerous physical properties, such as glass transition temperature,[3−11] molecular mobility,[12−16] diffusion of small, low molar mass tracer molecules,[17,18] phase behavior and morphology,[19−21] permeability,[22] moisture absorption,[23] electrical properties,[24] molecular orientations,[2,25−28] film stability, and dewetting.[29]

In particular, the crystallization of polymers in confined geometries has attracted widespread interest in recent years.[2,27,28,30−33] Similar to the altered glass transition temperatures of amorphous polymers in ultrathin films, the crystallization behavior observed in ultrathin films and block copolymer domains often differs significantly from the behavior found for the bulk. For instance, a preferred chain orientation, retarded lamellar growth rates, and lower degrees of crystallinity were observed in ultrathin films of various polymers. These effects were attributed to the presence of the two interfaces of the film with the substrate and the atmosphere. In block copolymers, the crystallization kinetics of poly(ethylene oxide) blocks confined to ∼8 nm lamellar spaces was found to be substantially slowed by the confinement between glassy blocks of PS.[31]

Sawamura et al. have reported that lamellar crystals grown isothermally in ultrathin films of isotactic polystyrene (iPS) on glass and carbon-coated substrates show significantly reduced growth rates compared to those of thicker films.[30a] The dependence of the normalized growth rate G_{norm} on film thickness d was shown by these authors to follow a $G_{norm} = (1 - \text{constant}/d)$ relationship. The constant was independent of crystallization temperature, molar mass of the polymer, and substrate material and was interpreted as the reptation tube diameter. The decrease in lamellar growth rate with decreasing film thickness was attributed to a reduction of the tube diameter near the substrate.

In our group ultrathin films of poly(di-*n*-hexylsilanes) on glass and quartz substrates have been investigated extensively.[2,27,28] Using UV absorption spectroscopy, we have shown that the molecular orientation, the crystallization kinetics, and the degree of crystallinity are strong functions of film thickness. The growth rates for isothermal crystallization were successfully fitted to the Avrami equation.[34] In particular, the transition from 3-D bulk crystallization to 1-D growth at high T_c and low film thicknesses and the absence of any detectable crystallinity for films thinner than 15 nm clearly showed that confinement into ultrathin films can substantially alter the crystallization behavior.[2,28]

As we have reported in a companion paper,[35] polarized infrared and fluorescence spectroscopic investigations on thin and ultrathin films of various poly(ethylene oxides) (PEO) on oxidized silicon showed that the polymer helices are preferentially oriented along the surface-normal direction in thin and ultrathin films. In addition, the crystallization rates were significantly reduced for films with thicknesses below ca. 100 nm.[36]

Here we report on the isothermal crystallization behavior of ultrathin films of PEO, as well as pyrene end-labeled PEO, on native oxide-covered silicon by hot stage AFM.[37−40] The lamellar growth rates, lamellar thicknesses, and melting ranges were systematically measured in situ on the level of single lamellae as a function of film thickness, crystallization temperature,

† Present address: University of Twente, Faculty of Chemical Technology and MESA+ Research Institute, Department of Materials Science and Technology of Polymers, P.O. Box 217, 7500 AE Enschede, The Netherlands.

* Corresponding authors. H.S.: phone ++31 53 489 3170; Fax ++31 53 489 3823; e-mail h.schonherr@ct.utwente.nl. C.W.F.: phone 650 723-4573; Fax 650 723-9780; e-mail curt@chemeng.stanford.edu.

10.1021/ma020686a CCC: $25.00
Published on Web 01/31/2003

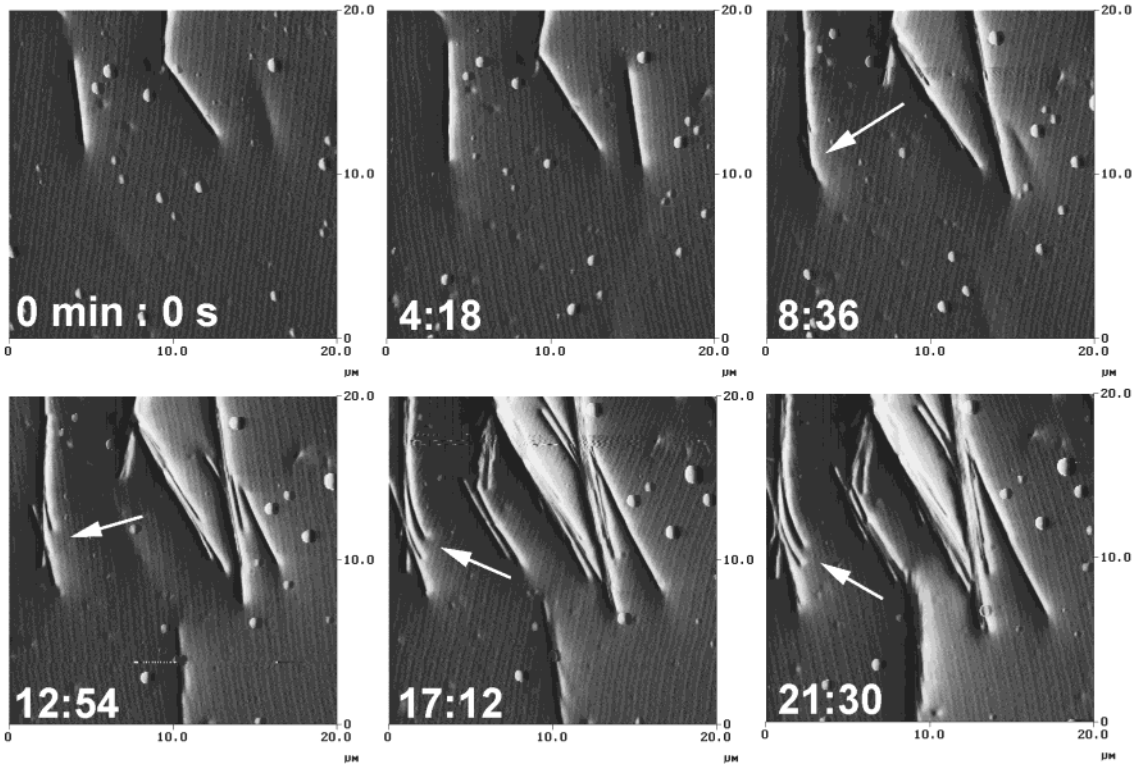

Figure 1. Sequence of TM-AFM amplitude images acquired at 53 °C on a film of PEOpy-49 on oxidized silicon (film thickness $d \approx 2.5\ \mu$m). The arrow points to an event of lamellar branching and splaying that results in the growth of a hedrite. The relative times are indicated.

and molar mass, and the data were fitted using established laws and theories, such as the Hoffman−Weeks extrapolation,[41,42] the Gibbs−Thomson equation,[43] and the Hoffman−Lauritzen theory.[44]

Experimental Section

Materials and Sample Preparation. Poly(ethylene oxide) (PEO, $M_w = 100\,000$ g/mol, Polysciences), pyrene end-labeled PEO (PEOpy, M_w (relative to PS): 49 340 g/mol ($M_w/M_n = 2.06$), 28 930 g/mol ($M_w/M_n = 1.91$), 10 800 g/mol ($M_w/M_n = 1.03$)),[35] and chloroform (Mallinckrodt) were used without further purification. The PEO materials are denoted PEO-100, PEOpy-49, PEOpy-29, and PEOpy-11, respectively. Thin films of PEO were prepared by spin-coating filtered solutions of PEO in chloroform onto argon plasma cleaned single-side or double-side polished silicon wafers, as described in ref 35. After the film preparation, the films were dried for at least 24 h in a vacuum. Thicknesses were determined by ellipsometry and by AFM profilometry.[35]

Tapping Mode Atomic Force Microscopy (TM-AFM). The TM-AFM data were acquired with a NanoScope III multimode AFM operated in tapping mode (Digital Instruments (DI), Santa Barbara, CA) using microfabricated silicon tips/cantilevers (Nanosensors, Wetzlar, Germany). AFM images were captured at elevated temperatures using a custom-built hot stage (vide infra) in ambient or dry argon atmosphere. Height, phase, and amplitude images were collected simultaneously using a set point ratio of 0.6−0.7; the rms amplitude of the cantilever vibration had to be increased by a factor of 2−3 compared to measurements in air in order to achieve stable imaging conditions. The images shown here were subjected to a first-order plane-fitting procedure to compensate for sample tilt and, if needed, a zeroth-order flattening. The home-built AFM hot stage, which is based on a dc powered Peltier element, and the temperature calibration have been described previously.[45]

Results

The morphology of isothermally crystallized PEO in thin and ultrathin films on oxidized silicon depends on the average film thickness. While films with thicknesses on the order of tens of micrometers exhibit spherulitic growth,[37,38] films with thicknesses in the 15−300 nm range show growth of individual lamellar crystals that are exclusively viewed in flat-on projection.[35,40,45] The latter lamellae are reminiscent of the classic work of Kovacs et al.[46] Hot stage AFM can be conveniently used to follow the crystallization of PEO in real time at a lamellar level, as shown in Figures 1 and 2. In the 2.5 μm thick film (Figure 1) lamellae grow preferentially in edge-on orientation, while in the 200 nm film (Figure 2) the lamellae are found *exclusively* in flat-on projection.

The edge-on PEOpy-49 lamellae depicted in Figure 1 start to branch and splay apart during the crystallization process, as indicated by the arrow. This process would eventually lead to the formation of hedrites[47] and finally spherulites.[48] In Figure 2, the growth of several lamellar crystals in flat-on projection and the action of growth spirals, which are caused by screw dislocations,[49,50] at the surface of a thin film of PEOpy-49 are shown. According to Bassett et al., the screw dislocations can be the origin of the lamellar branching, which is seen in orthogonal projection in Figure 1. The growth of quasi-hexagonal lamellae in thin and ultrathin films of PEO and pyrene end-labeled PEO was observed for *all* molar masses studied.

The growth rates of these lamellae proceeded linearly in time (Figure 3) and decreased only when lamellae began to impinge. Thus, for the low nucleation densities achieved by our self-seeding techniques, the growth rates of PEO and PEOpy can be measured accurately

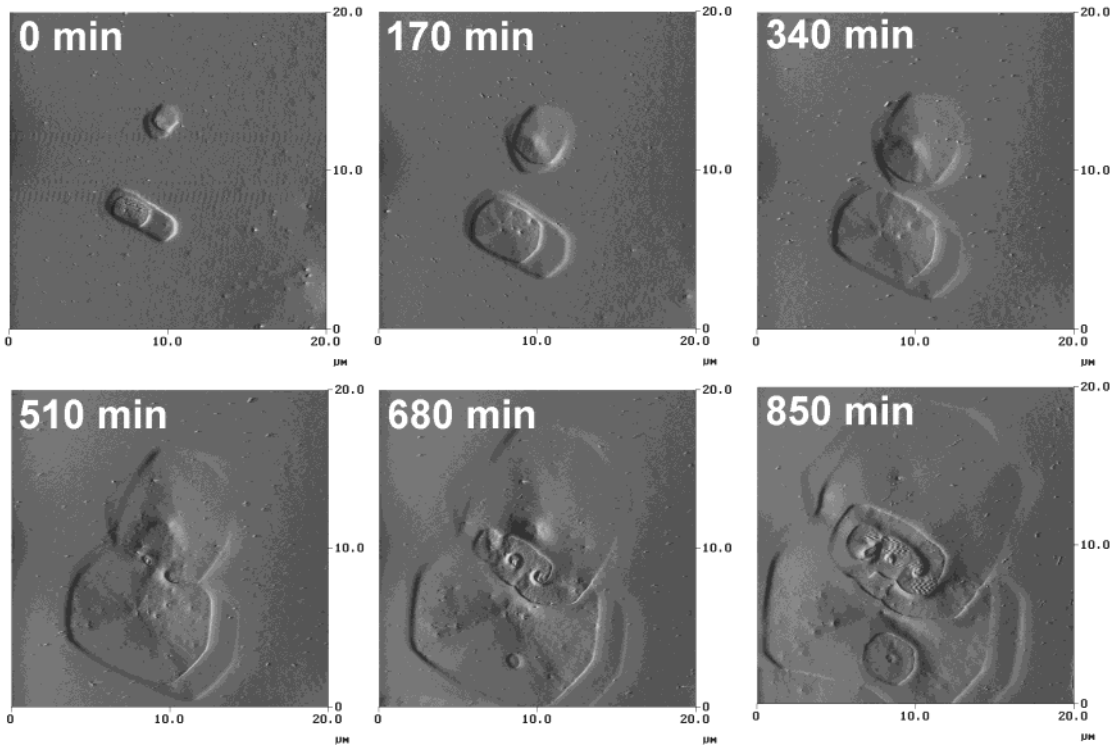

Figure 2. Sequence of TM-AFM amplitude images acquired at 58 °C on a film of PEOpy-49 on oxidized silicon (film thickness d = 200 nm). These images are frames 1, 20, 40, 60, 80, and 100 of a real-time movie of 100 images. The relative times are indicated.

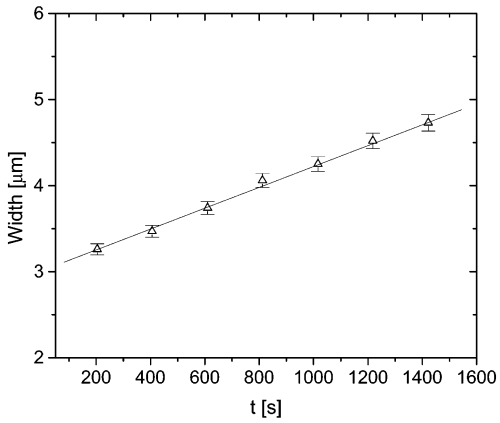

Figure 3. Width of a PEOpy-49 lamella in a 200 nm film on oxidized silicon as measured at 55 °C as a function of crystallization time. These AFM data allow one to calculate the linear lamellar growth rate from the slope.

in situ using hot stage AFM. The accessible range of growth rates is broad enough to allow one to perform a detailed analysis of the crystallization kinetics (vide infra).[51] Unlike the situation for films thicker than 5−10 μm, the presence of the AFM tip/cantilever close to the film surface has a negligible effect on the surface temperature in thin and ultrathin films.[45] The observation of constant linear growth rates suggests that the previously reported discontinuous growth of lamellae in spherulites is caused by competition among the different lamellae at the growth front.[37−39]

In Figure 4, the lamellar growth rates measured for PEO-100 and PEOpy-49 films with different thicknesses are summarized. The data for the lower M_w PEOpy materials look very similar (vide infra). The dependence of lamellar growth rates on temperature is comparable to that for conventional polymer bulk crystallization where the rates increase in first approximation exponentially with decreasing temperature for low undercoolings (Figure 4d). It is also obvious that the film thickness has a substantial effect on the magnitude of the rates.[35,36,40] The thinnest films show the lowest growth rates, while the differences between the 200 nm and the thicker films are negligible within errors. The film thickness dependence of the normalized growth rate for PEOpy-49 at 56 °C is shown in Figure 4c. For film thicknesses below ca. 200−500 nm, the magnitude of the growth rate begins to decrease markedly to a value less than 10−15% of its bulk value for films with thicknesses between ca. 15 and 100 nm. As shown in Figure 4d for films with approximately the same average thickness, the growth rates at the same undercooling is smaller for the higher molar mass PEO materials. However, if one takes the accuracy of the temperature calibration, the error in the determination of the equilibrium melting point $T_m°$, and the slight differences in film thickness into account, it becomes clear that the effect of different molar mass is small.

Lamellar thicknesses L were estimated from the pitch of the numerous growth spirals observed in AFM images of the PEO films, as depicted in Figure 5. A direct measurement of the step height between melt and lamellar crystal was not possible due an artifact: The height image in tapping mode AFM corresponds to a constant amplitude image. Since the melt damps the oscillation of the cantilever much more than the lamellae, the height measured in cross-sectional plots is highly inaccurate. In fact, this artifact results in AFM height images in which the lamellae *appear* depressed (Figure 6a). We only observed elevated lamellae for film thicknesses in which the lamellar thickness exceeds the average film thickness (Figure 6b). It cannot be excluded a priori that the increased density of the crystalline lamellae with respect to the amorphous melt may cause

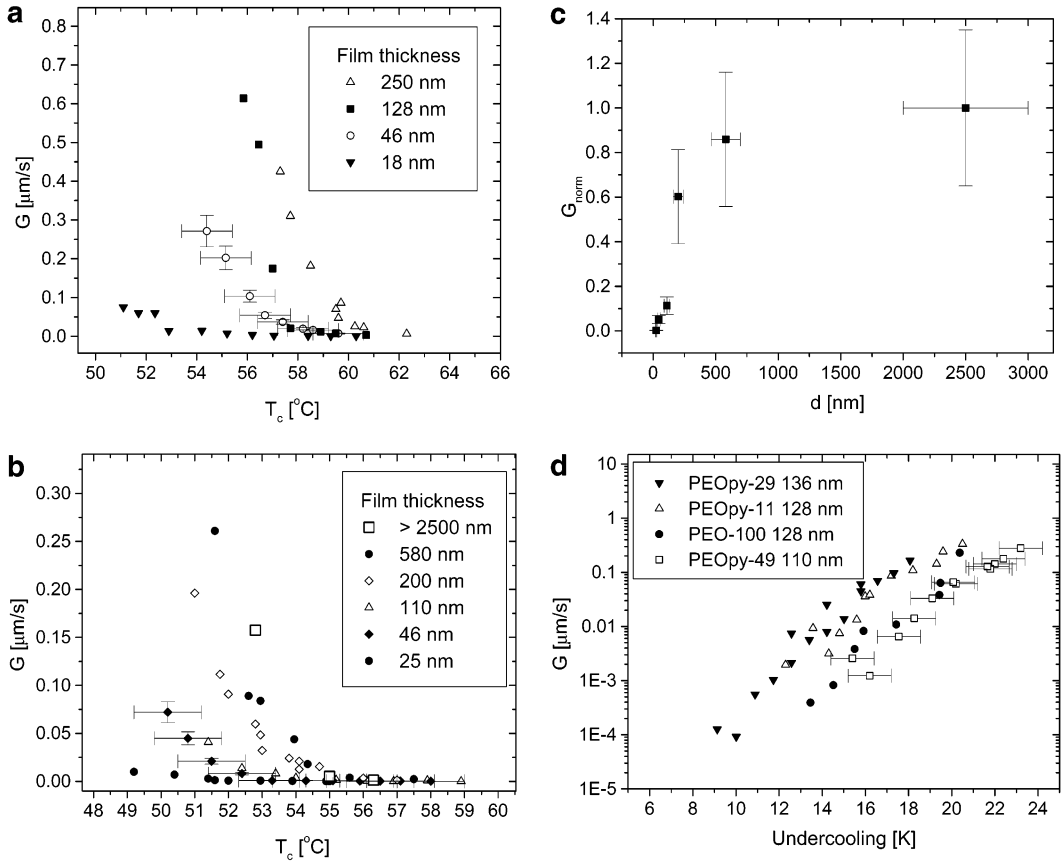

Figure 4. (a) Growth rate G as a function of crystallization temperature T_c for different film thicknesses of PEO-100 on oxidized silicon. (b) G as a function of T_c for different film thicknesses of PEOpy-49. (c) Growth rates of PEOpy-49 at 56 °C normalized to the growth rate of the thickest film as a function of film thickness. (d) Logarithmic plot of growth rates of various PEO and PEOpy films with similar thicknesses vs undercooling.

them to sink into the melt. However, our AFM images showed that the crystals remain stationary at the film−air interface for films thinner than 1 μm and that the lamellae are always at least partially covered with a thin film of melt (see also Figure 6a). Further, this observation can be corroborated by the observation of crystallization of this thin layer in the form of lamellar growth spirals due to screw dislocations (compare Figure 2 and Figure 5) or in the form of radiating lamellar crystals when the samples were more rapidly cooled to lower temperatures. Since the AFM tip penetrates through a thin layer of melt on top of the lamellae, the step height of growth spirals corresponds to the lamellar thickness L and *not* the long period.

In Figure 7 we have plotted the lamellar thicknesses for various films of the different PEO materials as a function of inverse undercooling. In agreement with the literature, the dependence of lamellar thicknesses on the inverse undercooling is linear.[52] The linear fits with boundary condition $L\ (1/\Delta T = 0) = 0$ yield satisfactory results. The data show that the lamellar thicknesses are not significantly affected by the molar mass; in fact, the data suggest that the lamellae for the lowest molar mass polymer may be slightly thinner for the same inverse undercooling. Moreover, the lamellar thicknesses do not vary significantly with film thickness (data not shown).

As mentioned, for most thicknesses of PEO films we have observed that the lamellae appear to be lower in height compared to the melt. This artifact also hampered the possible observation of the well-known depletion zones at the growth fronts of lamellar crystals.[37−39,47] Only in some cases we have observed a depletion zone in the thinnest films studied. The lamellae in the 18 nm film of PEOpy-49 depicted in Figure 6b (lower image) possess a clear depletion zone around the perimeter of the crystals. On the basis of this observation, we assume that a depletion zone exists for all film thicknesses; thus, the *actual* film thickness at the growth front is thinner than the mean film thickness. For the discussion of the dependence of the lamellar growth rate on film thickness the presence of a depletion zone is of crucial importance, as this would lower the actual film thickness compared to the average thickness considerably (vide infra).

The equilibrium melting point $T_m°$ was estimated independently by a Hoffmann−Weeks extrapolation (Figure 8)[41,42] as well as a plot based on the Gibbs−Thomson equation (eq 1, Figure 9).[43]

$$T_m = T_m°\left(1 - \frac{2\sigma_e}{L\Delta H}\right) \tag{1}$$

where T_m and $T_m°$ are the melting temperature and the equilibrium melting temperature, respectively, σ_e denotes the interfacial energy of the fold surface, L is the lamellar thickness, and ΔH is the heat of fusion.

The results for the equilibrium melting points as determined by both methods are summarized in Table 1. For instance for PEO-100, both methods yield the same result of $T_m° = 77$ °C to within the accuracy of the data and the extrapolation. This is an excellent agreement with the literature data ($T_m° = 76$ °C).[54,55] The values for the PEOpy materials are lower due to the effect of the chain ends and polydispersity for

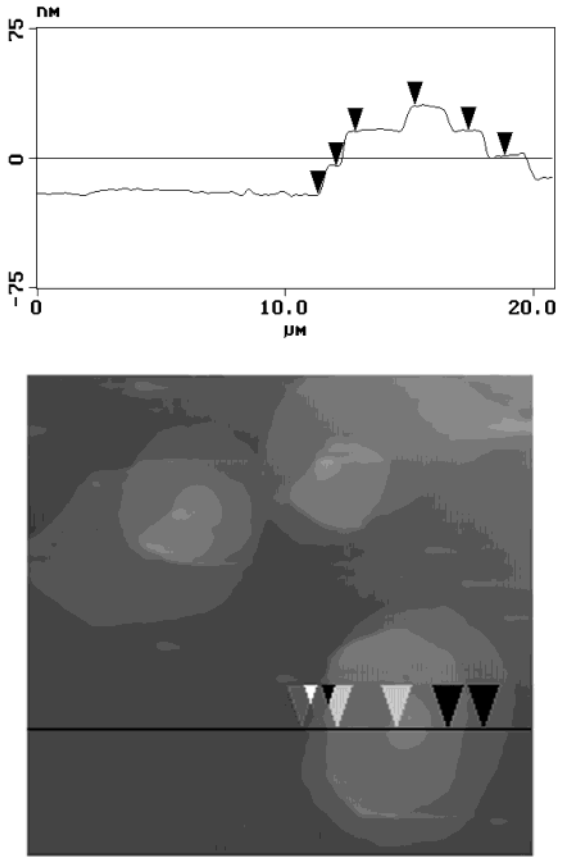

Figure 5. Section analysis of TM-AFM height images acquired on growth spirals on top of a fully crystallized PEO-100 lamella in a 46 nm film on oxidized silicon (T_c = 58 °C). The vertical distances between the markers are 16.5, 14.9, and 14.9 nm.

PEOpy-49 and PEOpy-29.[53] In addition, the presence of the pyrene end groups very likely affects the degree of perfection of the lamellar crystals for temperatures where chain ends are partially incorporated into the lamellar interior. Similar to the lamellar thicknesses, the melting point data did *not* show a significant dependence on film thickness (Figure 8b), which is in contrast to a recent report by Kim et al.[54,55]

The linear fits of the Gibbs−Thomson plot also yield the surface free energy of the relevant fold planes σ_e. If we take the limited number of data points due to the limited number of well-developed growth spirals into account, the comparison with the literature data shows again a good agreement (Table 2).

The known dependencies and descriptions for lamellar thicknesses, melting, and crystallization temperatures for bulk samples seem to be similarly valid for ultrathin films. The equilibrium melting points and surface free energies of the fold planes, as shown above, do not seem to be significantly affected by the confinement of the PEO into ultrathin films. By contrast, the growth rate data shown in Figure 4 suggest drastic effects of the confinement on the crystallization kinetics. To identify the possible origins for these effects and understand the observed growth rate depression in ultrathin films better, we have fitted the growth rate data to the Hoffman−Lauritzen theory.[44] Marentette and Brown have shown that the crystallization of PEO in the bulk can be well described using this approach.[55]

The linearized Hoffman−Lauritzen plots[56] for the different PEO materials are shown in Figure 10a−d for various film thicknesses. In agreement with this polymer crystallization theory, we observe a linear dependence for all materials and all film thicknesses. Despite the differences in growth rates due to confinement (vide supra), the linearized plots according to the Hoffman−Lauritzen theory can describe *all* the data. The slopes for data acquired for the PEO-100 and PEOpy-49 materials seem to be practically invariant with the film thickness. For the lower molar mass PEOpy materials, we observe a possible trend to decreasing slopes with decreasing film thickness.

The results obtained from fitting the data according to the Hoffman−Lauritzen theory can be compared with the data based on fits of the Gibbs−Thomson equation (Table 2). We observe in general a favorable agreement. There seems to be no obvious trend of the surface free energy of the fold plane σ_e as a function of film thickness; the mean values decrease slightly with molar mass of the polymer, which is in accordance with the literature.[43] Furthermore, the mean values (averaged over all film thicknesses) for σ_e of 28, 28, 22, and 23 erg/cm^2 for PEO-100, PEOpy-49, PEOpy-29, and PEOpy-11, respectively, agree very well with the literature data on bulk crystallization as reported by Marentette and Brown.[55] These authors reported a surface free energy of the fold plane of 29 erg/cm^2 for PEO with a molar mass of 100 kg/mol based on polarized optical microscopy measurements and stated 14, 20, and 26 erg/cm^2 for PEO with molar masses of 110, 145, and 594 kg/mol, respectively, for recalculated literature data.[55] The favorable comparison of our data to the literature shows that hot stage AFM can indeed provide accurate quantitative data that may be used to extract various kinetic and thermodynamic parameters.

Discussion

We have imaged in situ the melting and isothermal crystallization of individual lamellae in thin and ultrathin films of PEO and pyrene end-labeled PEO on oxidized silicon using hot stage AFM. On the basis of these AFM data (lamellar thicknesses L, lamellar growth rates G, and melting temperatures T_m), we have applied the Hoffman−Weeks extrapolation, the Gibbs−Thomson equation, and the Hoffman−Lauritzen theory and showed that we obtain reasonable values for the equilibrium melting point and the surface free energy of the fold surface. Except for a retarded growth rate for decreasing average film thicknesses, we have *not* observed any deviations from the conventional crystallization behavior of PEO.

The retarded growth rates for ultrathin films caused a constant offset of the linearized Hoffman−Lauritzen plots, but the slope of the curve remains unaffected to a first approximation (Figure 10a−d). Apparently, the transport term of the linearized Hoffman−Lauritzen equation does not correct appropriately for the transport properties in ultrathin films, i.e., either the activation energy for reptation across the melt−crystal interface or the temperature at which molecular motion ceases (T_∞) was underestimated. By using appropriate values for U^* or T_∞, all curves fall onto a single curve. As mentioned, the melting points as measured by AFM did not show any measurable dependence on film thickness.

If we assume that the confinement into ultrathin films alters the glass transition temperature T_g of PEO, the transport term can be corrected. It is physically reasonable to assume an increase in T_g since the oxidized

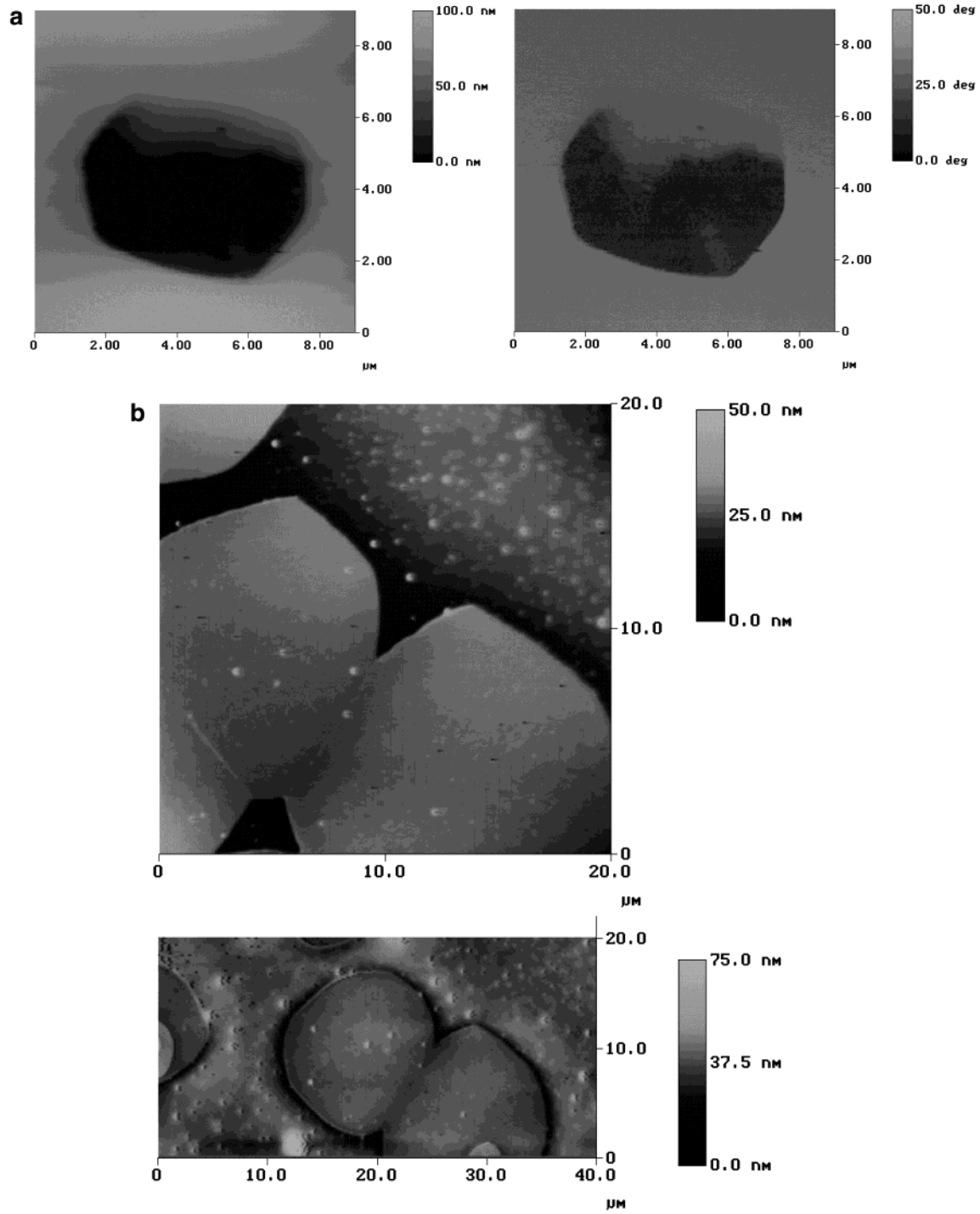

Figure 6. (a) Dual TM-AFM height (left) and phase images (right) of growing PE0-100 lamella in 46 nm film on oxidized silicon imaged at 58 °C. The top part of the lamellae is clearly covered by a featureless material which has the same phase contrast as the melt. (b) Two TM-AFM height images acquired on 18 nm films of PEOpy-11 at 43 and 41 °C (bottom) show that the height of the growing lamella exceeds that of the melt. On the lower image a depletion zone at the growth front is visible.

silicon provides an interactive surface. Interactive substrates have been reported to lead to an increase in glass transition temperature of supported ultrathin polymer films.[4−6,10,11] An increase in T_g would also increase T_∞ and hence shift the curves for thinner films toward the curve for the thickest films. If we attribute the altered crystallization kinetics in the ultrathin films exclusively to an increase in T_g and assume that the Hoffman−Lauritzen theory is an appropriate description, we can extract T_g as a function of film thickness. In Figure 11 we have plotted the corresponding values for T_g for ultrathin films of PEO-100 and the different PEOpy derivatives on oxidized silicon. In agreement with work by Forrest et al.,[5a] the change in T_g of supported films does not seem to be a strong function of molar mass.

The presence of a depletion zone at the growth front complicates the analysis of the film thickness dependence considerably. Since we are unable to detect the very likely existing depletion zones for most film thicknesses due to an artifact in the determination of the height differences between melt and growing lamella (vide supra), we cannot determine the film thickness at the growth front quantitatively. Hence, the actual film

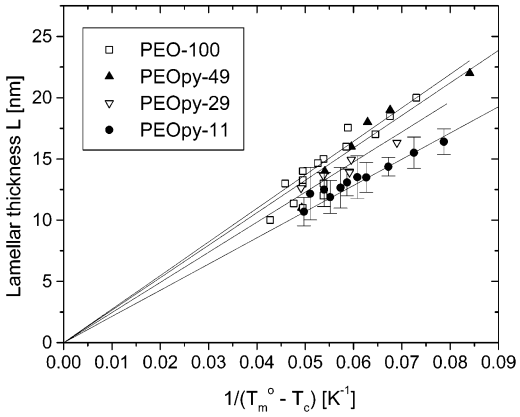

Figure 7. Plot of lamellar thicknesses vs inverse undercooling for all PEO materials studied. The data were acquired by section analysis of TM-AFM height images of growth spirals observed on films with thicknesses between 110 and 135 nm.

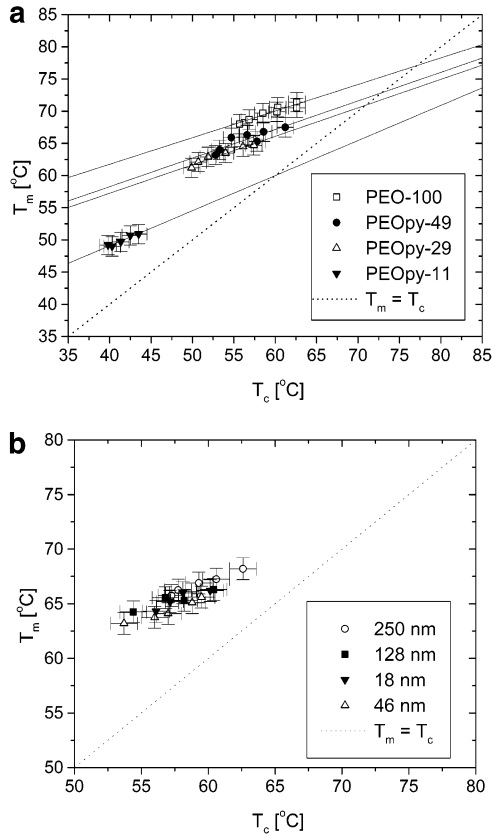

Figure 8. (a) Hoffman−Weeks plot[41,42] for films of all PEO materials with thicknesses between 110 and 135 nm. (b) Hoffman−Weeks plot[41,42] for PEO-100 for films with variable thickness. To within the accuracy of the experiment there is no systematic trend of T_m vs T_c as a function of film thickness.

thickness at the growth front may be substantially less than the stated average thickness, such as indicated on the abscissa in Figure 11. Thus, the T_g values inferred for ultrathin films of PEO from this rough analysis cannot be a priori related to the mean film thickness.

If we plot the growth rate, normalized to the rate at a thickness where confinement effects are very small to nonexistent, as a function of inverse film thickness, we obtain a much stronger dependence of the growth rate depression with film thickness compared to the iPS reported by Sawamura et al.[30a] Instead of a (1 − constant/d) dependence, we find an exponential dependence in the form of exp(1 − constant*/d) (Figure 12), in agreement with the Avrami analysis of FT-IR spectroscopy data.[35]

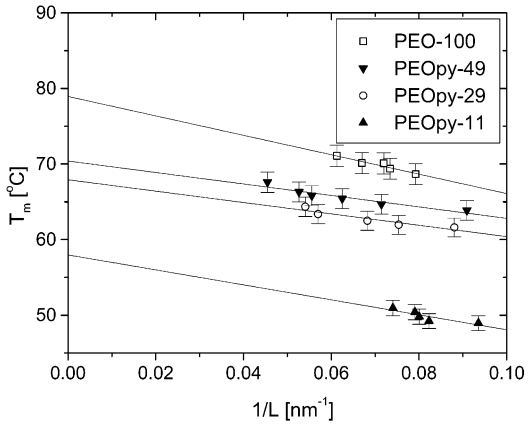

Figure 9. Gibbs−Thomson plot for all PEO materials studied in films with thicknesses between 110 and 135 nm.

Table 1. Equilibrium Melting Points Determined by Linear Hoffman−Weeks Extrapolation and Linear Regression Analysis of the Gibbs−Thomson Plot

	T_m° [°C]	
polymer	Hoffman−Weeks[41,42]	Gibbs−Thomson[43]
PEO-100	77 ± 2	76 ± 2
PEOpy-49	73 ± 2	70 ± 2
PEOpy-29	71 ± 2	68 ± 2
PEOpy-11	60 ± 2	58 ± 2

Table 2. Surface Free Energy of Fold Surface As Determined by Linear Regression Analysis of the Gibbs−Thomson Plot and Fitting of the Data Based on the Hoffman−Lauritzen Theory

		surface free energy of fold surface σ_e [erg/cm^2]	
polymer	film thickness [nm]	Gibbs−Thomson fit[43]	Hoffman−Lauritzen fit[44,55]
PEO-100	250		24.8 ± 4.0
	128	32.6 ± 3.0	26.5 ± 4.0
	46		28.4 ± 4.0
	18		32.2 ± 4.0
PEOpy-49	580		26.2 ± 4.0
	200		26.9 ± 4.0
	110	29.2 ± 3.0	29.3 ± 4.0
	46		27.8 ± 4.0
	25		28.4 ± 4.0
PEOpy-29	550		18.5 ± 4.0
	136	29.0 ± 3.0	24.0 ± 4.0
	38		25.1 ± 4.0
	24		19.2 ± 4.0
	22		21.7 ± 4.0
PEOpy-11	128	36.1 ± 6.0	17.1 ± 4.0
	38		20.0 ± 4.0
	20		31.5 ± 4.0
	14		24.9 ± 4.0

From the combined AFM, FT-IR, and fluorescence spectroscopic data discussed in this and the companion paper,[35] it is evident that the confinement of PEO into ultrathin films affects the morphology of the films, the orientation of the polymer chains, and the orientation of the lamellar crystals. The presence of the substrate−film and the film−atmosphere interface is likely responsible for the altered behavior of PEO in these ultrathin films. However, most changes become significant at distances that are larger and often much larger than the perturbation of the chain conformation as inferred by various authors ($2R_g$).[57] For our materials, the radii of gyration are ca. 10.8, 7.6, 5.8, and 3.5 nm for PEO-100, PEOpy-49, PEOpy-29, and PEOpy-11,

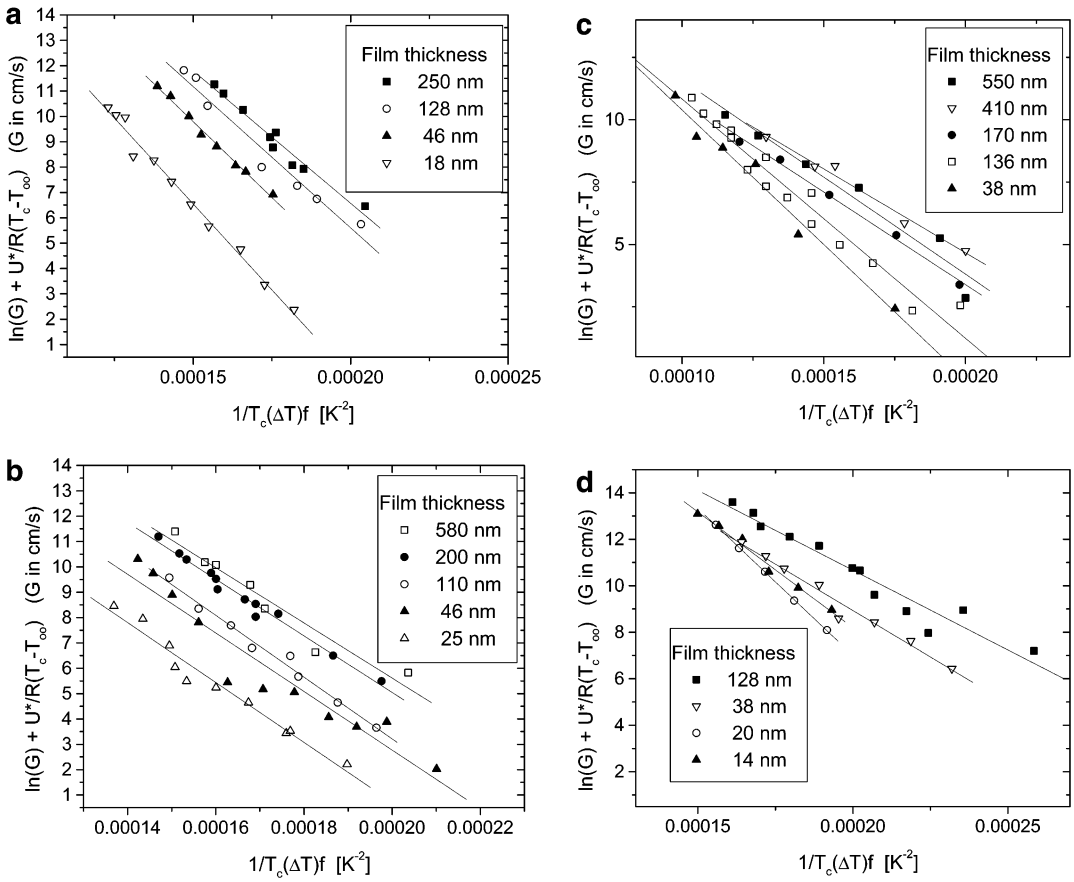

Figure 10. Linearized Hoffman−Lauritzen plots for crystallization of (a) PEO-100, (b) PEOpy-49, (c) PEOpy-29, and (d) PEOpy-11 for various film thicknesses.

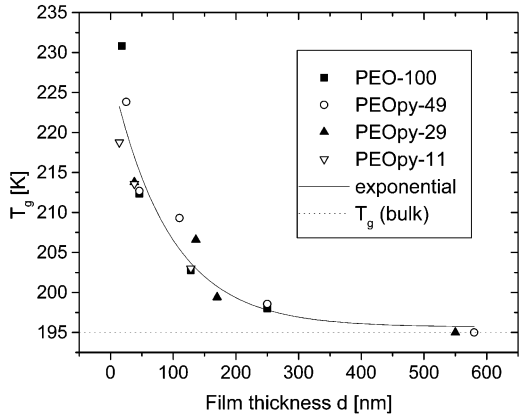

Figure 11. Values for T_g derived from a correction of the transport term of the linearized Hoffman−Lauritzen equation vs average film thickness. The curves of PEO-100 and PEO-11 have been shifted by addition of a constant to overlap with the most complete data sets which were obtained for PEOpy-49 and PEOpy-29. Note that the film thickness refers to average film thickness; the actual film thickness at the growth front may be substantially less due to the presence of a depletion zone (see text). The first-order exponential has been fitted to all data points and serves to guide the eyes.

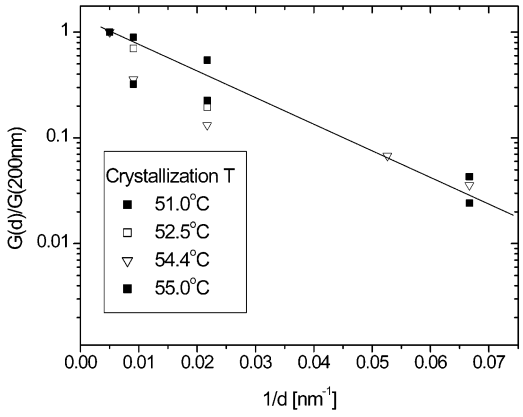

Figure 12. Normalized growth rates of PEOpy-49 as measured at different temperatures vs inverse film thickness. Note that we observe an exponential dependence unlike Sawamura et al., who observed a linear dependence for iPS on glass.[30]

respectively, which means that the interface is screened for all thicknesses studied.[35]

We can at this point only speculate that the same mechanisms that cause an increase in T_g for ultrathin films on interactive surfaces and T_g depressions on noninteractive substrates[11] also operate in the ultrathin films of PEO studied here. Related to the postulated increase in glass transition temperature is a decrease in polymer mobility, which in turn slows down the lamellar growth rates.

Summary

We have studied the isothermal crystallization of ultrathin films of poly(ethylene oxide) (PEO), as well as pyrene end-labeled PEO, on native silicon using hot stage atomic force microscopy. Lamellar growth rates, lamellar thicknesses, and melting ranges were measured as a function of film thickness, crystallization temperature, and molar mass. On the basis of the linear Hoffman−Weeks extrapolation, the Gibbs−Thomson equation, and the Hoffman−Lauritzen theory, we show that the crystallization of PEO in thin and ultrathin

films is governed by the same laws as the bulk crystallization. The equilibrium melting points and surface free energies of the fold surfaces agree quantitatively with literature data for bulk crystallization. The substantial decrease of lamellar growth rates is attributed to an increase in glass transition temperature of PEO ultrathin films on silicon oxide and the concomitant reduction of molecular mobility. This increase in glass transition temperature is consistent with an adjustment of the transport term in the framework of the Hoffman−Lauritzen theory.

Acknowledgment. The authors thank Larry E. Bailey for his contribution in building the AFM hot stage. H.S. gratefully acknowledges financial support by the Deutsche Akademischer Austauschdienst (DAAD) in the framework of the "Hochschulsonderprogramm III" and the NSF MRSEC Center on Polymer Interfaces and Macromolecular Assemblies (CPIMA) under DMR 9808677.

References and Notes

(1) *Physics of Polymer Surfaces and Interfaces*; Sanchez, I. C., Ed.; Butterworth-Heinemann: Boston, 1992.
(2) Frank, C. W.; Rao, V.; Despotopoulou, M. M.; Pease, R. F. W.; Hinsberg, W. D.; Miller, R. D.; Rabolt, J. F. *Science* **1996**, *273*, 912 and references cited therein.
(3) Keddie, J. L.; Jones, R. A. L.; Cory, R. A. *Europhys. Lett.* **1994**, *27*, 59.
(4) Keddie, J. L.; Jones, R. A. L.; Cory, R. A. *Faraday Discuss.* **1994**, *98*, 219.
(5) Forrest, J. A.; Dalnoki-Veress, K.; Dutcher, J. R. *Phys. Rev. E* **1997**, *56*, 5705. (b) Forrest, J. A.; Mattson, J. *Phys. Rev. E* **2000**, *61*, R53.
(6) Prucker, O.; Christian, S.; Bock, H.; Rühe, J.; Frank, C. W.; Knoll, W. *Macromol. Chem. Phys.* **1998**, *199*, 1435.
(7) DeMaggio, G. B.; Frieze, W. E.; Gidley, D. W.; Zhu, M.; Hristov, H. A.; Yee, A. F. *Phys. Rev. Lett.* **1997**, *78*, 1524.
(8) Jones, R. A. L. *Curr. Opin. Colloid Interface Sci.* **1999**, *4*, 153.
(9) Kim, J. H.; Jang, J.; Zin, W. C. *Langmuir* **2000**, *16*, 4064. (b) Kim, J. H.; Jang, J.; Zin, W. C. *Langmuir* **2001**, *17*, 2703.
(10) van Zanten, J. H.; Wallace, W. E.; Wu, W. L. *Phys. Rev. E* **1996**, *53*, R2053.
(11) Fryer, D. S.; Nealey, P. F.; de Pablo, J. J. *Macromolecules* **2000**, *33*, 6439. (b) Torres, J. A.; Nealey, P. F.; dePablo, J. J. *Phys. Rev. Lett.* **2000**, *85*, 3221. (c) Fryer, D. S.; Nealey, P. F.; de Pablo, J. J. *J. Vac. Sci. Technol. B* **2000**, *18*, 3376.
(12) Frank, B.; Gast, A. P.; Russell, T. P.; Brown, H. R.; Hawker, C. *Macromolecules* **1996**, *29*, 6531.
(13) Zheng, X.; Rafailovich, M. H.; Sokolov, J.; Strzhemechny, Y.; Schwarz, S. A.; Sauer, B. B.; Rubinstein, M. *Phys. Rev. Lett.* **1997**, *79*, 241.
(14) Zheng, X.; Sauer, B. B.; van Alsten, J. G.; Schwarz, S. A.; Rafailovich, M. H.; Sokolov, J.; Rubinstein, M. *Phys. Rev. Lett.* **1995**, *74*, 407.
(15) Russell, T. P.; Kumar, S. K. *Nature (London)* **1997**, *386*, 771.
(16) Lin, E. K.; Kolb, R.; Satija, S. K.; Wu, W.-L. *Macromolecules* **1999**, *32*, 3753.
(17) Tseng, K. C.; Turro, N. J.; Durning, C. J. *Phys. Rev. E* **2000**, *61*, 1800. (b) Tseng, K. C.; Turro, N. J.; Durning, C. J. *Polymer* **2000**, *41*, 4751.
(18) Hall, D. B.; Torkelson, J. M. *Macromolecules* **1998**, *31*, 8817.
(19) Krausch, G.; Dai, C.-A.; Kramer, E. J.; Marko, J. F.; Bates, F. S. *Macromolecules* **1993**, *26*, 5566.
(20) Meuse, C. W.; Yang, X.; Yang, D.; Hsu, S. L. *Macromolecules* **1992**, *25*, 925. (b) Tao, H.-J.; Meuse, C. W.; Yang, X.; MacKnight, W. J.; Hsu, S. L. *Macromolecules* **1994**, *27*, 7146.
(21) Fasolka, M. J.; Banerjee, P.; Mayes, A. M.; Pickett, G.; Balazs, A. C. *Macromolecules* **2000**, *33*, 5701.
(22) Pfromm, P. H.; Koros, W. J. *Polymer* **1995**, *36*, 2379.
(23) Beck Tan, N. C.; Wu, W. L.; Wallace, W. E.; Davis, G. T. *J. Polym. Sci., Part B: Polym. Phys.* **1998**, *36*, 155.
(24) Liang, T.; Makita, Y.; Kimura, S. *Polymer* **2001**, *42*, 4867.
(25) Hietpas, G. D.; Allara, D. L. *J. Polym. Sci., Part B: Polym. Phys.* **1998**, *36*, 1247.
(26) Bartczak, Z.; Argon, A. S.; Cohen, R. E.; Kowalewski, T. *Polymer* **1999**, *40*, 2367.
(27) Despotopoulou, M. M.; Frank, C. W.; Miller, R. D.; Rabolt, J. D. *Macromolecules* **1995**, *28*, 6687. (b) Despotopoulou, M. M.; Miller, R. D.; Rabolt, J. D.; Frank, C. W. *J. Polym. Sci., Part B: Polym. Phys.* **1996**, *34*, 2335.
(28) Despotopoulou, M. M.; Frank, C. W.; Miller, R. D.; Rabolt, J. F. *Macromolecules* **1996**, *29*, 5797.
(29) Reiter, G. *Europhys. Lett.* **1993**, *23*, 579.
(30) Sawamura, S.; Miyaji, H.; Izumi, K.; Sutton, S. J.; Miyamoto, Y. *J. Phys. Soc. Jpn.* **1998**, *67*, 3338. (b) Sutton, S. J.; Izumi, K.; Miyaji, H.; Miyamoto, Y.; Miyatashi, S. *J. Mater. Sci.* **1997**, *32*, 5621.
(31) Zhu, L.; Cheng, S. Z. D.; Calhoun, B. H.; Ge, Q.; Quirk, R. P.; Thomas, E. L.; Hsiao, B. S.; Yeh, F.; Lotz, B. *Polymer* **2001**, *42*, 5829 and references cited therein.
(32) Jing, S.; Qiao, C.; Tian, S.; Ji, X.; An, L.; Jiang, B. *Polymer* **2001**, *42*, 5755.
(33) Reiter, G.; Sommer, J.-U. *Phys. Rev. Lett.* **1998**, *80*, 3771. (b) Reiter, G.; Sommer, J.-U. *J. Chem. Phys.* **2000**, *112*, 4376.
(34) Avrami, M. *J. Chem. Phys.* **1939**, *7*, 1103. (b) See ref 28.
(35) Schönherr, H.; Frank, C. W. *Macromolecules* **2003**, *36*, 1188.
(36) In the course of writing these manuscripts a similar study has been published by Dalnoki-Veress et al. which describes the reduction of crystallization rates for PEO thin films on silicon and gold substrates as studied by quartz crystal microbalance and video optical microscopy (Dalnoki-Veress, N.; Forrest, J. A.; Massa, M. V.; Pratt, A.; Williams, A. *J. Polym. Sci., Part B: Polym. Phys.* **2001**, *39*, 2615). The complementary results reported by these authors are in good agreement with our data.
(37) Pearce, R.; Vancso, G. J. *Macromolecules* **1997**, *30*, 5843. (b) Pearce, R.; Vancso, G. J. *Polymer* **1998**, *39*, 1237.
(38) Schultz, J. M.; Miles, M. J. *J. Polym. Sci., Part B: Polym. Phys.* **1998**, *36*, 2311.
(39) Studies on polymer crystallization close to room temperature (without active control of the specimen temperature) have been reported: e.g. McMaster, T. J.; Hobbs, J. K.; Barham, P. J. Miles, M. J. *Probe Microsc.* **1997**, *1*, 43.
(40) Schönherr, H.; Waymouth, R. M.; Hawker, C. J.; Frank, C. W. *ACS Polym. Mater.: Sci. Eng.* **2001**, *84*, 453.
(41) Hoffman, J. D.; Weeks, J. J. *J. Res. Nat. Bur. Stand.* **1962**, *66A*, 13.
(42) Recently, Marand et al. have shown that the established linear Hoffman−Weeks extrapolation leads to a significant underestimation of the equilibrium melting temperature (Marand, H.; Xu, J.; Srinivas, S. *Macromolecules* **1998**, *31*, 8219). In this work we have utilized the linear extrapolation, and hence our result is likely an underestimate. Taking the limited number of available data points into account, we were unable to perform the correct nonlinear extrapolation.
(43) For discussion of various aspects of polymer crystallization see e.g.: (a) Wunderlich, B. *Macromolecular Physics*; Academic Press: New York, 1973, 1976, 1980; Vols. 1, 2, 3. (b) Woodward, A. E. *Atlas of Polymer Morphology*; Hanser: Munich, 1989. (c) Bassett, D. C. *Principles of Polymer Morphology*; Cambridge University Press: Cambridge, 1981. (d) Strobl, G. *Polymer Physics*; Springer: Heidelberg, 1997. (e) Gedde, U. *Polymer Physics*, 1st ed.; Kluwer Academic Publishers: Dordrecht, 1995. (f) *Crystallization of Polymers*; Dosiere, M., Ed.; NATO ASI Series; Kluwer Academic Publishers: Dordrecht, 1993.
(44) Lauritzen, J. I., Jr.; Hoffman, J. D. *J. Res. Natl. Bur. Stand.* **1960**, *64A*, 73. (b) Clark, E. J.; Hoffman, J. D. *Macromolecules* **1984**, *17*, 878. (c) Hoffman, J. D. *Polymer* **1983**, *24*, 3. (d) Lauritzen, J. I., Jr.; Hoffman, J. D. *J. Appl. Phys.* **1973**, *44*, 4340. (e) Hoffman, J. D.; Miller, R. L. *Macromolecules* **1989**, *22*, 3502.
(45) Schönherr, H.; Bailey, L. E.; Frank, C. W. *Langmuir* **2002**, *18*, 490.
(46) Kovacs, A. J.; Straupe, C.; Gonthier, A. *J. Polym. Sci., Polym. Symp. Ed.* **1977**, *59*, 31.
(47) Geil, P. H. *Polymer Single Crystals*; Wiley-Interscience: New York, 1963; Chapter 3.
(48) Vaughan, A. S.; Bassett, D. C. *Comprehensive Polymer Science*; Pergamon Press: New York, 1989; Vol. 2, p 415.
(49) Bassett, D. C. *Philos. Trans. R. Soc. London, A: Phys. Sci. Eng.* **1994**, *348*, 29.
(50) Keller, A. In *Growth and Perfection of Crystals*; Doremus, R. H., Roberts, B. W., Turnbull, D., Eds.; Wiley: New York, 1958; p 499. (b) Norton, D. R.; Keller, A. *Polymer* **1985**, *26*, 704. (c) Reference 43c. (d) Bassett, D. C. *Macromol. Symp.* **1999**, *143*, 11.
(51) For the specific case of thin films of PEO, the AFM data acquisition is limited to lamellar growth rates of ca. 0.5−1.0

μm/s and slower. This estimate is based on the growth of a lamellar crystal over the distance of a typical scan size of 20 μm within the time elapsed to capture six subsequent images using the following parameters: resolution = 128 pixels/line, 16 lines scanned, scan rate = 2.5−5.0 Hz.

(52) Barham, P. J.; Chivers, R. A.; Keller, A.; Martinez-Salazar, J.; Organ, S. J. *J. Mater. Sci.* **1985**, *20*, 1625.

(53) An estimate of the expected melting point depression based on treating the chain ends as impurities and recalculating the molar masses relative to PS to the nominal molar masses leads to ΔT_m of ca. 2, 3, and 4 K for PEOpy-49, PEOpy-29, and PEOpy-11, respectively, relative to PEO-100 (Young, R. J.; Lovell, P. A. *Introduction to Polymers*, 2nd ed.; Chapman & Hall: London, 1991; p 288; with heat of fusion per repeat unit ΔH_{ru} = 8.7 kJ/mol).[55]

(54) Kim, J. H.; Jang, J.; Zin, W.-C. *Macromol. Rapid Commun.* **2001**, *22*, 386.

(55) Marentette, J. M.; Brown, G. R. *Polymer* **1998**, *39*, 1405.

(56) According to the Hoffman−Lauritzen theory,[43,44] the lamellar growth rate G can be expressed as $G = G_0 \exp[-U^*/R(T_c - T_\infty)] \exp(-K_g/T_c\Delta T f)$ with U^* the energy barrier for reptation across the melt−crystal interface (U^* = 29.3 kJ/mol),[55] T_c the crystallization temperature, T_∞ the temperature at which molecular motion relevant for the crystallization process ceases, defined as $T_g - 30$ K, where the glass transition temperature was 195 K,[55] K_g the nucleation constant (defined below), the undercooling $\Delta T = T_m^o - T_c$ (as a function of the equilibrium melting point T_m^o), and a dimensionless correction factor f, which corrects for decreasing heat of fusion at lower temperatures. The correction factor f is written as $f = 2T_c/(T_m^\circ + T_c)$. The nucleation constant K_g is a function of the regime of crystallization through parameter j (see below), the crystalline molecular thickness in growth direction b_0 (b_0 = 4.62 Å for (120) face),[55] the lateral surface interfacial free energy σ (taken as 24.24 erg/cm^2),[55] the fold surface interfacial free energy σ_e, the Boltzmann constant k, and the heat of fusion ($\Delta H = 2.66 \times 10^9$ erg/cm^3):[55] $K_g = 2jb_0\sigma\sigma_e T_m^\circ/k\Delta H$. Regime I growth ($j = 2$) refers to the situation where the secondary nucleation step controls the linear growth rate and regime II growth ($j = 1$) refers to the multiple nucleation case, while regime III growth ($j = 2$) characterizes prolific nucleation; see refs 44 and 43e, p 178). On the basis of a comparison of the temperature and molar mass range investigated, we tentatively assign our data to regime III growth in accordance with ref 55.

(57) Simulation work by various methods suggested disturbed single chain properties for polymer molecules near a wall in the melt. (a) Ten Brinke, G.; Ausserre, D.; Hadziioannou, G. *J. Chem. Phys.* **1988**, *89*, 4374. (b) Kumar, S. K.; Vacatello, M.; Yoon, D. Y. *J. Chem. Phys.* **1988**, *89*, 5207. (c) Bitsanis, I.; Hadziioannou, G. *J. Chem. Phys.* **1990**, *92*, 3827. Recent experimental findings by Jones et al. (Jones, R. A. L.; Kumar, S. K.; Ho, D. L.; Briber, R. M.; Russell, T. P. *Nature (London)* **1999**, *400*, 14) suggest that the conformation of the macromolecules in ultrathin films is retained parallel to the surface to within the error of the small-angle neutron scattering data. Kraus et al. observed a significant distortion of the chain conformation by diffuse neutron scattering (Kraus, J.; Müller-Buschbaum, P.; Kuhlmann, T.; Schubert, D. W.; Stamm, M. *Europhys. Lett.* **2000**, *49*, 210).

MA020686A